

Glass transition improvement in epoxy/graphene composites

Hélio Ribeiro · Wellington M. Silva · Marco-Tulio F. Rodrigues ·
Juliana C. Neves · Roberto Paniago · Cristiano Fantini · Hálten D. R. Calado ·
Luciana M. Seara · Glaura Goulart Silva

Received: 28 February 2013 / Accepted: 24 May 2013 / Published online: 10 August 2013
© Springer Science+Business Media New York 2013

Abstract Graphene oxide nanoplatelets (GO) were prepared from expanded graphite (EG) and functionalized with triethylenetetramine (GO-TETA). The GO-TETA consisted of a few layers of graphene (~4–6 layers), as determined by atomic force microscopy and Raman spectroscopy. X-ray photoelectron spectroscopy showed that the TETA was covalently linked to the GO in the GO-TETA sample. Epoxy composites based on the diglycidyl ether of bisphenol A with TETA as a hardener and with 0.5–3.0 wt% additions of EG and GO-TETA were investigated. The results showed that the addition of the nanofillers led to an increase of ~20 °C in the glass transition temperature. A slight increase in the ratio of the elastic modulus/hardness of the nanocomposites was observed by nanoindentation tests carried out at a depth range of 300 nm–1.3 µm; these tests indicated a tendency of increased fracture toughness. Microindentation had an enhancement of 40 % in hardness for the 1 wt% composite with GO-TETA relative to the corresponding value for the neat epoxy.

Electronic supplementary material The online version of this article (doi:10.1007/s10853-013-7478-3) contains supplementary material, which is available to authorized users.

H. Ribeiro · W. M. Silva · M.-T. F. Rodrigues ·
J. C. Neves · H. D. R. Calado · G. G. Silva (✉)
Departamento de Química, Universidade Federal de Minas
Gerais, Belo Horizonte, Minas Gerais, Brazil
e-mail: glaura@qui.ufmg.br

R. Paniago · C. Fantini
Departamento de Física, Universidade Federal de Minas Gerais,
Belo Horizonte, Minas Gerais, Brazil

L. M. Seara
Centro de Microscopia, Universidade Federal de Minas Gerais,
Belo Horizonte, Minas Gerais, Brazil

Introduction

There has been a great deal of interest in carbon nanotubes and graphene-based composites, especially related to the remarkable electronic and mechanical properties of these new carbon materials [1–4].

Graphene in its pure form is not compatible with either organic solvents or polymers and does not form homogeneous composites [3–5]. One strategy used to improve the dispersion of graphene nanosheets in a polymer matrix is the oxidation and functionalization of the carbonaceous surface, which increases polymer wettability. Graphite oxide (GO) has been mainly produced by the Brodie [6], Staudenmaier's [7], and Hummers' [8] methods. Furthermore, several works have been done using Hummers' modified methods [3–5, 9, 10]. The surface functional groups of GO are epoxides, alcohols, carboxylic acids, and other ketone groups; the contents of these functional groups can vary significantly, depending on the starting material and oxidative conditions. A recent study [11] has shown that GO, produced by the Hummers method, is composed of functionalized graphene sheets decorated by strongly bound oxidative debris. This is similar to the polycyclic aromatic acids on oxidized multiwall carbon nanotubes [12]. When a suspension of the as-produced GO is treated with an aqueous solution of NaOH, the consequence is a black aggregate that separates out [13]. A possible additional functionalization route of GO is through reaction of the COOH groups with thionyl chloride (SOCl₂) [5, 9], followed by an additional reaction with amine groups [14].

Polymer/graphene nanocomposites possess superior mechanical, thermal, and electrical properties compared to neat polymers, as has been previously reviewed by Kuila et al. [3] and Potts et al. [4]. The glass transition

temperature (T_g) of amorphous polymers is one of the most important parameters to consider when designing technological applications. At temperatures just above T_g , a non-crystalline polymer material behaves rubbery, or as a viscous fluid, depending on the molecular weight and degree of crosslinking. Below T_g , a bulk polymer becomes a glass that is more or less brittle (with remaining flexibility provided by side-chains) depending on the structure [15]. Because epoxies are thermosetting materials, the T_g is considered the upper limit of service temperature for epoxy-based systems and, for that, increases in T_g are associated with enhancements in the thermal stability of the polymers [16, 17].

Low nanofiller loading has been reported to cause large shifts in the glass transition temperature (T_g) of thermoplastic-based nanocomposites; for example, a shift of +30 °C with just a 0.05 % loading of functionalized graphene sheets was observed for nanocomposites with poly(methylmethacrylate) [16]. For the epoxy systems, the increase in the T_g in the reported results has frequently been less than 20 °C [18–22], and occasionally, a decrease in T_g values has been reported [23, 24]. Hu et al. [18] observed that 0.50 vol% of amino-functionalized graphene with 4,4-diaminodiphenyl sulfone (DDS) added to an epoxy can increase the T_g by 12 °C. Zaman et al. [20] achieved an increase of 14 °C of T_g to 2.5 wt% graphene nanoplatelets functionalized with 4,4'-methylene diphenyl diisocyanate/epoxy system; whereas, Bortz et al. [19] obtained an maximum increase of 17 °C of loss modulus peak for a 0.5 wt% GO nanosheets/epoxy matrix. Martin-Gallego et al. [21] reported increases in the T_g of 21 and 40 °C [25] resulting from the addition of GO nanosheets to a photocured epoxy at 1 and 1.5 wt%, respectively.

Putz et al. [22] discussed the influence of the addition of non-modified carbon nanotubes on the epoxy glass transition over a range of cross-linking densities. They demonstrated that a competition between the epoxy network disruption and the creation of an interphase can limit the effects T_g increase for highly cross-linked epoxies. However, when modified carbon-based nanofillers are employed, surface functionalization can take part in the curing reaction, resulting in advantageous changes in the structure of the interphase and allowing an increase in the T_g even for highly cross-linked epoxies [22].

Nanoindentation allows for the mechanical probing of a material surface at a penetration depth of approximately 10 nm–10 μ m [26]. This technique can assist in the optimization of the material composition, structure and processing. A major advantage of nanoindentation is the ability to study small specimens, as there is good agreement between the results of nanoindentation and those obtained from other mechanical properties tests, such as elastic modulus and hardness [27].

The hardness and the elastic modulus are obtained by analyzing the load–displacement data recorded during the loading–unloading indentation cycles. The hardness is defined as the indentation load divided by the projected contact area (A_c) of the indentation. For a Berkovich indenter (having a triangular diamond pyramid shape), A_c is a function of the contact depth. The elastic modulus can be obtained from the slope of the initial portion of the unloading curve and is usually calculated as proposed by Oliver and Pharr [28]. The elastic modulus calculated in this way can be regarded as “apparent” because this model neglects the viscoelasticity of the epoxy. This model can be used without introducing significant error because the testing time is lower than the characteristic creep time of the material [26]. There have been several reports of nanoindentation studies for epoxy nanocomposites [27, 29–32].

Lee et al. [27] applied an indentation load to attain a depth of 3–4 μ m with epoxy/carbon nanofiber composites and observed very good agreement between the elastic moduli obtained from tensile tests and nanoindentation tests, with a maximum difference of 2 %. Li et al. [30] investigated an indentation depth of 1 μ m on epoxy/coiled carbon nanotube samples and observed a 40 % increase in the elastic modulus following the addition of 5 wt% nanofiller.

The range of the nanofillers' effect in the composite mechanical properties was studied by complementary tests that were performed by microindentation. Vickers microhardeners have been considered a reliable tool in viscoelastic material characterization [33]. It has been shown that the absence of elastic recovery along the diagonals justifies the use of Vickers indentation as a convenient tool to probe rigid polymeric materials such as epoxy [34].

The objective of the present work was to produce increases in the T_g with epoxy-based nanocomposites. For this purpose, two types of nanofillers were selected: commercial expanded graphite and synthesized TETA-functionalized graphene nanosheets. First, a full characterization of both the EG and GO-TETA was performed, and the glass transition and morphology of the nanocomposites were investigated. Nanoindentation tests at various depths and microindentation were carried out to probe the effect of the nanofillers on the mechanical properties of the composites.

Experimental

Materials

The materials used in this work were expanded graphite (EG) from “Nacional de Grafite” Company (Brazil), conc.

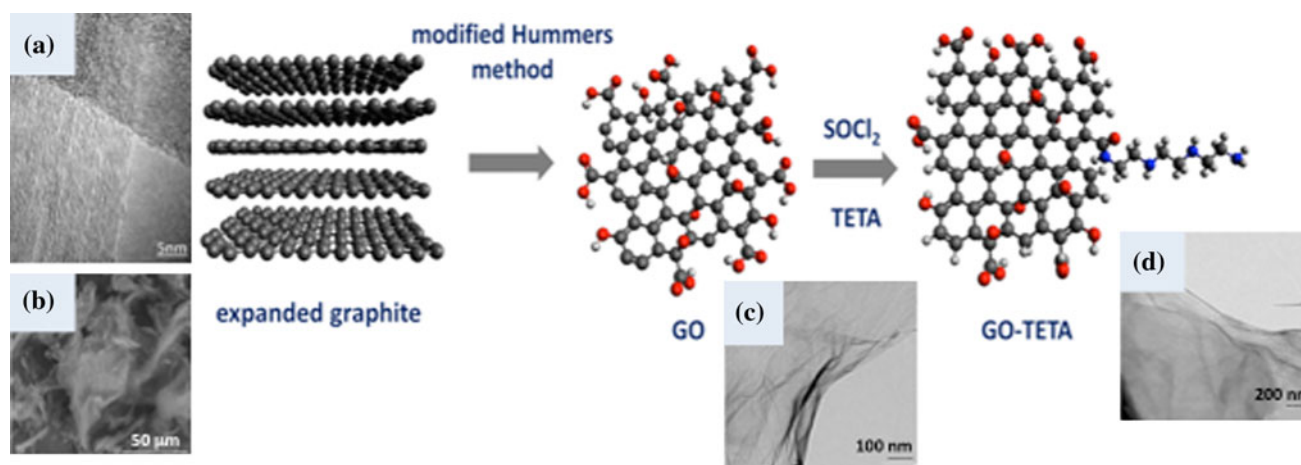


Fig. 1 Schematic of the functionalization of GO-TETA from expanded graphite. **a, b** TEM micrograph and SEM micrograph for EG; **c** TEM micrographs for graphene oxide nanosheets (GO) and **d** TETA-modified graphene oxide nanosheets (GO-TETA)

H₂SO₄ (Merck), KMnO₄ (VETEC), sodium nitrate (VETEC), *N*-methyl-pyrrolidone (Aldrich) and a diglycidyl ether of bisphenol A (DGEBA)-based epoxy resin (MC130) with an amine hardener based on triethylenetetramine (TETA; DEH 24), which was supplied by Epoxyfiber Company.

Methodology

Oxygenated groups were introduced to the surfaces of EG using a modified Hummers method [8] to produce graphene oxide nanosheets (GO). In a typical process, 1.00 g of expanded graphite powder was oxidized with 0.50 g sodium nitrate in 70 mL of concentrated H₂SO₄. This mixture was placed in an ice bath, and 3.00 g of KMnO₄ was gradually added; distilled water was added after stirring for 8 h. Oxidation with 10 % w/w H₂O₂ was carried out while stirring for 1 h. Following oxidation, the mixture was centrifuged, filtered under a vacuum through a 0.45-μm polytetrafluoroethylene membrane and then washed until a neutral pH was obtained. The filtered product was dried in a hot oven at 100 °C for 12 h.

For functionalization, 120 mL of freshly distilled SOCl₂ was added to 0.30 g of the oxidized graphene nanosheets (GO). The mixture was heated to 70 °C under reflux for 24 h, after which SOCl₂ was extracted by distillation and 120 mL of TETA was added. The reagent mixture was then heated to 120 °C under reflux for 72 h, after which the mixture was cooled to room temperature, centrifuged and dispersed in a beaker containing 300 mL of anhydrous ethanol to remove any TETA adsorbed to the surface of the GO. The remaining solution was vacuum-filtered and washed thoroughly with anhydrous ethanol to insure that any adsorbed material was removed; TETA is highly soluble in this solvent. The filtered material was dried at

100 °C for 12 h and named GO-TETA. A schematic of the process of functionalization of GO-TETA is shown in Fig. 1.

Nanocomposites with concentrations of 0.5, 1.0, and 3.0 wt% EG and GO-TETA investigated in this study were produced following the same procedure.

First, the carbon nanomaterials were mixed manually in epoxy resin without hardener to obtain a good suspension. This suspension was then added to a three-roll mill (Exakta) for final high shear mixing, using a gap size between ceramic rolls of 5 μm and a speed of 22 in the 1st roll, 66 in the 2nd roll, and 200 rpm in the 3rd roll. The suspension was rolled approximately ten times to complete homogenization. The suspensions were collected, mixed manually with hardener and cured under a vacuum for 1 h at 40 °C and then for four additional hours at 120 °C.

Characterization

To evaluate the degree of exfoliation for both GO and GO-TETA, for each sample, suspensions with ~0.05 mg/mL (diluted from a 1 mg/mL stock solution) in *N*-methylpyrrolidone were dispersed for 30 min in an ultrasonic bath and then dropped onto Si substrates and porous carbon film-coated copper grids, followed by drying and characterization with atomic force microscopy (AFM) or transmission electron microscopy (TEM), respectively. TEM micrographs were obtained on an FEI TECNAI G2 microscope with a 200 kV accelerating voltage.

AFM micrographs were obtained on an MFP-3D-SA SPM microscope (Asylum Research, CA, USA) under ambient conditions (relative humidity ~50 %, temperature ~20 °C). AFM was performed in tapping mode to characterize the morphology by recording topographical

images; silicon cantilevers (Olympus AC240TS) with a spring constant of $\sim 2 \text{ Nm}^{-1}$ (between 0.5 and 4.4 Nm^{-1}) and a typical resonance frequency of $\sim 70 \text{ kHz}$ (between 50 and 90 kHz) were used.

Thermogravimetric analysis measurements were obtained using an SDT 2960 TGA from TA Instruments. The samples were analyzed from 30–1000 °C at a heating rate of 5 °C/min under a synthetic air atmosphere flowing at 100 mL/min.

XPS spectra were obtained at room temperature on a VG Scientific Escalab 220-ixL system. The base pressure in the vacuum chamber was 2.0×10^{-10} mbar, which removes molecules adsorbed on the sample surface. A Mg anode was used to generate X-rays with a $K\alpha$ line at 1487 eV. XPS spectra between 0 and 1000 eV (stretched spectra) were obtained at 1 eV steps, and high-resolution spectra with 0.1 eV steps were obtained in the peak photoemission regions for the C 1s, N 1s, and O 1s electrons. The electron energy analyzer operated in large area mode ($\varnothing = 4 \text{ mm}$) with a pass energy of 50 eV for the stretched spectra and 20 eV for the high-resolution spectra. Each spectrum was adjusted using a combination of Gaussian and Lorentzian functions.

Micro-Raman experiments were performed using a Dilor XY spectrometer with a backscattering geometry and equipped with a liquid nitrogen-cooled CCD detector. Samples were resolved on an OLYMPUS BH-2 optical microscope with a $100\times$ objective using the 514.5 nm Ar–Kr laser line and a power of 1 mW to avoid any spectral changes due to sample heating. Spectra were collected at three different points for each sample.

SEM micrographs of the nanocomposites were obtained on a Quanta 200 model FEG-FEI 2006 microscope operating under vacuum with a 10-kV accelerating voltage. To study the dispersion of graphene, the epoxy nanocomposites were cut to a thickness of 40 nm using an ultramicrotome, and the films were deposited on a 200 mesh porous carbon film-coated copper grid.

Differential scanning calorimetry (DSC) measurements were performed on a 2920 model calorimeter from TA Instruments. The nanocomposite samples were analyzed according to ASTM standard D 3418–82 [35].

Nanoindentation tests were performed using an Asylum Research Nanoindenter (CA, USA) equipped with a Berkovich tip. Composites were prepared using molds that were cured and cut to a thickness of 2–3 mm. The elastic moduli and hardness of the nanocomposites were obtained in a displacement-controlled mode, with an indent and withdraw rate of 30 nm/s. A total of 36 indentations on a $50 \times 50 \mu\text{m}$ area were made for each sample, with the average values reported. Four maximum depths were used: 50 nm, 300 nm, 600 nm, and 1.3 μm . The elastic moduli were calculated from the recorded load–displacement

curves according to the Oliver-Pharr Method [28]. Poisson's ratio for the thin films was assumed to be 0.33 for the calculation. The results obtained from these experiments were statistically evaluated by analysis of variance (ANOVA) and by Tukey's test. All tests were conducted with a significance level (α) of 0.05 evaluated with Minitab 15 statistical software.

Reicherter's Hardness tester was used for microindentation. Short specimens ($10 \times 10 \times 6 \text{ mm}$) of cured epoxies were cut and polished before measurement. The Vickers indenter tip was pushed 20 s into the specimen surface at an applied load of 2 N. The hardness value was measured immediately after indentation and 20 indentations were applied per sample to guarantee the accuracy of the evaluation. After removal of the load, the diagonal lengths of the indents were measured using a microscope and the average hardness was calculated. The elastic recovery in the direction of the diagonals was generally negligible or very small. Therefore, the measurement of diagonal lengths ($\sim 100 \mu\text{m}$ for neat epoxy for instance) gave valid hardness values for the epoxy systems (viscoelastic rigid polymers) [34].

Results and discussion

Characterization of graphene nanoplatelets

Figure 1a–d shows SEM and TEM micrographs for EG (a, b), GO (c), and GO-TETA (d). The commercial expanded graphite sample (EG) in Fig. 1a–b was exfoliated to provide a few layers of graphene chemically modified by oxidized groups (GO) and by TETA as shown in the schematic in Fig. 1. The GO-TETA sample shown observed in Fig. 1d is transparent and has a wrinkled, thin, paper-like morphology. TEM micrographs of the flakes of EG, as shown in Fig. 1a, indicate that they are composed of tenths to hundreds of graphitic layers.

Typical AFM micrographs for GO-TETA (as shown in Fig. 2a) were used to determine the thickness, which corresponds to the height in the cross-sectional profile (inset in Fig. 2a). AFM is frequently used to characterize graphene that is a few layers thick. The thickness of a single layer of graphene, obtained via AFM, in the literature is reported to range between 0.34 and 1.2 nm depending on any extension due to functionalization [5, 36].

The sample in Fig. 2a shows a height of 1.7 nm for the GO-TETA sample, corresponding to a maximum thickness of ~ 5 layers. Figure 2b shows a TEM image of GO-TETA sample with ~ 6 graphitic layers. Analysis of several AFM and TEM images lead to the conclusion that GO and GO-TETA have a distribution in the number of layers, with maxima between 4 and 6 layers. Moreover, significant

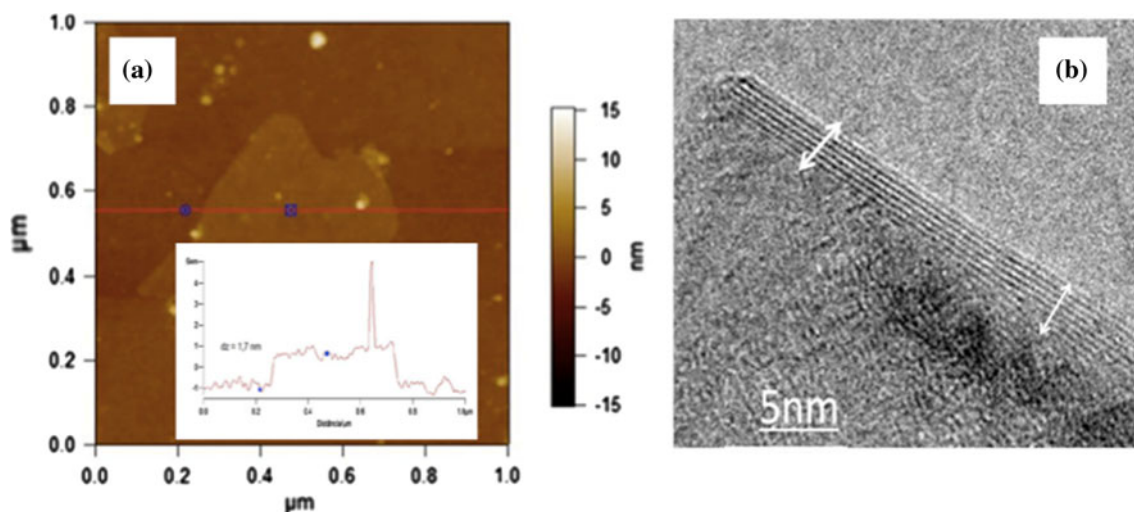
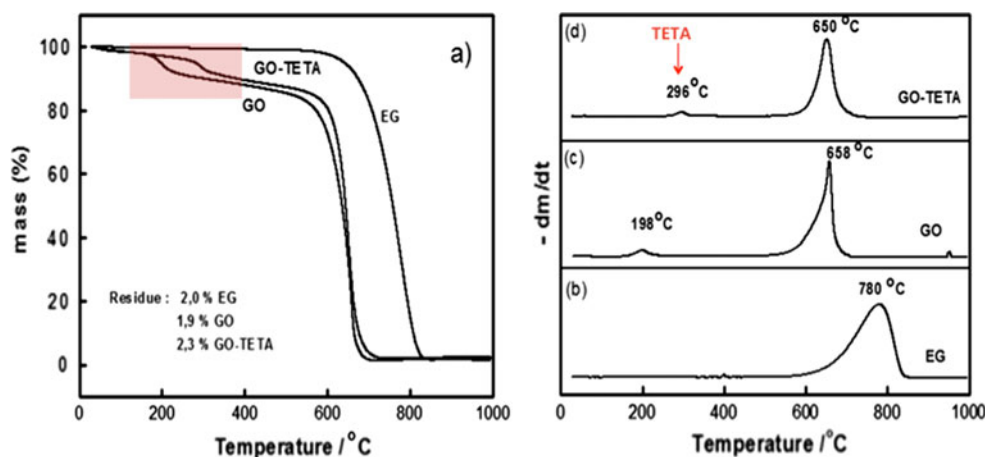


Fig. 2 **a** Representative tapping mode AFM micrograph for GO-TETA film and **b** high-resolution TEM image of the edge of GO-TETA showing approximately 6 graphitic layers

Fig. 3 **a** TG and **b–d** DTG curves for EG, GO, and GO-TETA samples. The TETA mass loss occurs at 296 °C and corresponds to 13 % in **(d)**



folding or overlapping was observed in the nanosheets. The lateral dimensions of the functionalized graphene ranged from several 100 nm to a few micrometers.

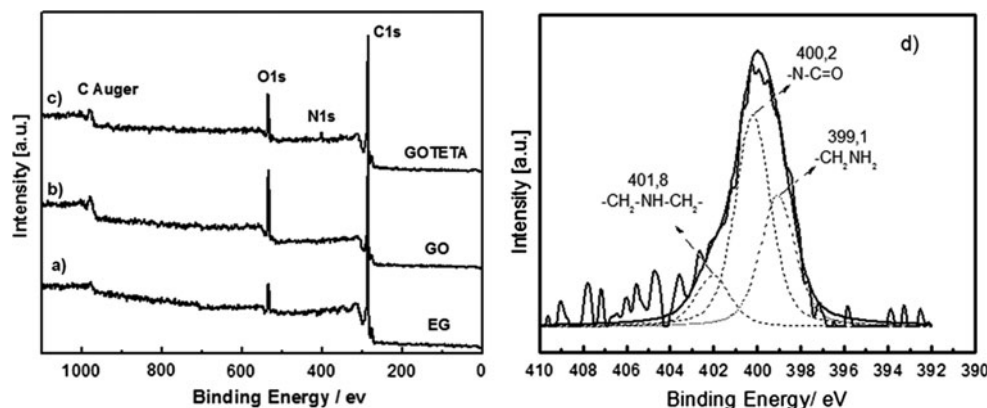
Raman Spectroscopy was applied to investigate the number of layers, as well as other properties of the graphene nanosheets [36–42]. Raman results and discussions are available in the Supporting Information. The range in the number of layers between ~4 and 6 as observed by AFM and TEM was corroborated by Raman analysis (Fig. 9 of the Supporting Information). The number of graphene layers that can promote an effective reinforcement will depend on the thickness of polymer chains in between the platelets as discussed by Young et al. [13]. Moreover, the lateral dimensions are critical [13] and they should not be compromised largely in the exfoliation process.

The percentage mass loss as a function of temperature (TG) and the derivative mass loss percentage (DTG) are

shown in Fig. 3a–d for EG, GO and GO-TETA, respectively. Most of the carbonaceous oxidation occurs approximately 655 °C for GO and GO-TETA and approximately 780 °C for EG due to an increase in exfoliation, cutting and structural defects in the functionalized graphene nanosheets compared to the expanded graphite [43]. A peak was observed at 198 °C in the DTG curve for GO due to a ~10 % mass loss of oxygenated functional groups (Fig. 3c). GO-TETA showed a mass loss of ~13 % approximately 296 °C (Fig. 3d) due to oxidative decomposition of the TETA functional groups [14, 44].

XPS spectra were obtained for the main elements of interest (C, O, and N) to determine the chemical composition of the carbonaceous materials [45–50]. Figure 4a–c shows the XPS survey spectra of the EG, GO, and GO-TETA samples. All samples show photoemission peaks for C 1s (~284.5 eV) and O 1s (~534.0 eV). Figure 10 (Supporting Information) exhibits the detailed C 1s and O

Fig. 4 XPS survey spectra for **a** EG, **b** GO, and **c** GO-TETA samples and **d** high-resolution XPS spectra obtained in the N 1s bonding energy region for GO-TETA



1s XPS spectra for the EG, GO, and GO-TETA samples and a discussion of these results is also available in the Supporting Information. N 1s photoemission peaks (~ 400.0 eV) were only observed in the GO-TETA spectra. The presence of an amide carbonyl group was identified in the N 1s spectrum (Fig. 4d), confirming the covalent attachment of TETA to the graphene layers in the GO-TETA sample. After adjusting the photoemission peaks, three significant contributions were identified, with binding energies in the range of 399.1–401.8 eV. Here, nitrogen atoms with a binding energy of 399.1 eV are attributed to primary amines ($-\text{CH}_2-\text{NH}_2$). Nitrogen atoms with a binding energy of ~ 400.2 eV correspond to amide carbonyl groups ($-\text{N}-\text{C}=\text{O}$), and nitrogen atoms with a binding energy of ~ 401.8 eV are attributed to secondary amines ($-\text{CH}_2-\text{NH}-\text{CH}_2-$) [45, 46].

Characterization of composite/graphene nanosheets

SEM micrographs of both the neat epoxy and the composites with EG and nanoplatelets of GO-TETA are shown in Fig. 5a–c. Figure 5 shows micrographs obtained for thin slices, which indicate that a better dispersion of the filler was likely obtained for the GO-TETA nanomaterial than for the expanded graphite. Figure 5b reveals a large agglomeration of EG, which leads to a disruption in the uniformity of the thin slice of the epoxy composite. Figure 5c confirms that good adhesion was obtained between the functionalized graphene and the epoxy. A schematic of the morphology observed in the SEM images is also showed in the bottom of Fig. 5. Although inspection of the SEM micrographs of Fig. 5a–c uncovers the benefits of graphene exfoliation and functionalization, studying a greater number of SEM samples prepared by both ultramicrotomy and fracture (Fig. 11 of the Supporting Information) showed some agglomerates and zones free of graphene nanoplatelets in all composite samples produced.

Representative DSC curves for the neat epoxy and the nanocomposites with concentrations of 0.5, 1.0 and

3.0 wt% EG and GO-TETA are shown in Fig. 6. The T_g reported is the average of three independent measurements to obtain significant results. The T_g for each sample was determined from the midpoint of the corresponding glass transition regions and is listed in Table 1 along with standard deviations of less than ± 1 °C. Figure 6 shows that the glass transition region is larger for the composites than for the neat epoxy, which is associated with the filler effect of broader the segmental motion range. However, the width of the glass transition region (between onset and offset) was of 11 °C on average for neat epoxy and maximum of 20 °C for composite samples. These width values for the glass transition region are within a range that allows an accurate determination of T_g , considering the triplicate measurements and the carefully performed analysis.

There is a clear increase in the T_g of 10–20 °C of the composites in respect to the neat epoxy for the two systems evaluated. Similar increases in the T_g were observed for the nanocomposites produced with an epoxy and different types of modified graphene [18–20], which establishes the present results as being among the best reported in the literature. However, it is important to note that the increases in the T_g were similar between EG and GO-TETA. Therefore, both types of fillers possessed a similar tendency to increase the glass transition temperature in the case of the materials and processes employed in this work. This similarity may be a consequence of the competition between the creation of an interphase and the disruption of cross-linking, as proposed by Putz et al. [22].

The GO-TETA was dispersed as nanosheets that were ~ 2 nm thick, while the EG platelets were more than 10 nm thick (Figs. 1, 2, 5). The GO-TETA can produce stronger interphase regions by covalently linking with the epoxy. However, the GO-TETA can also introduce a higher disturbance to the cross-linking mechanism, leading to a counterbalance in the desired effect of increasing the T_g .

Representative load–displacement curves for the nanoindentation tests and an AFM image of the nanoindentation mark are shown in Fig. 7a, b for the GO-TETA composite

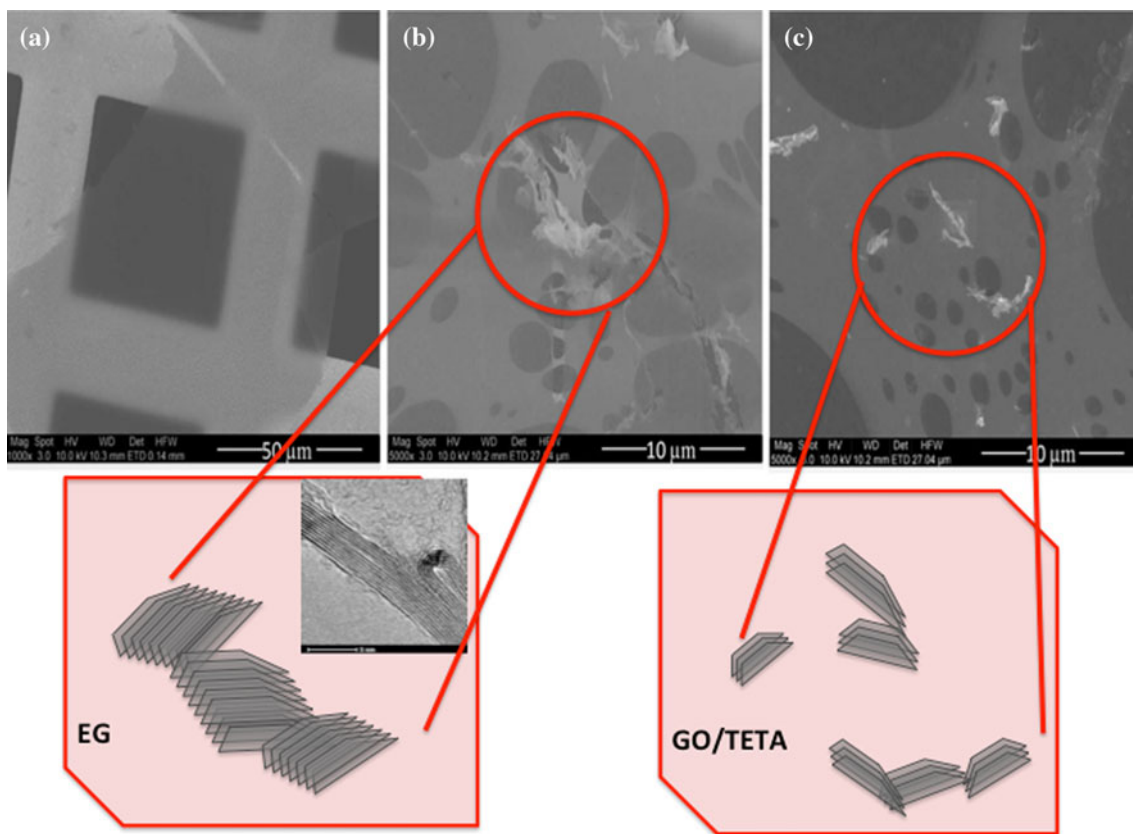
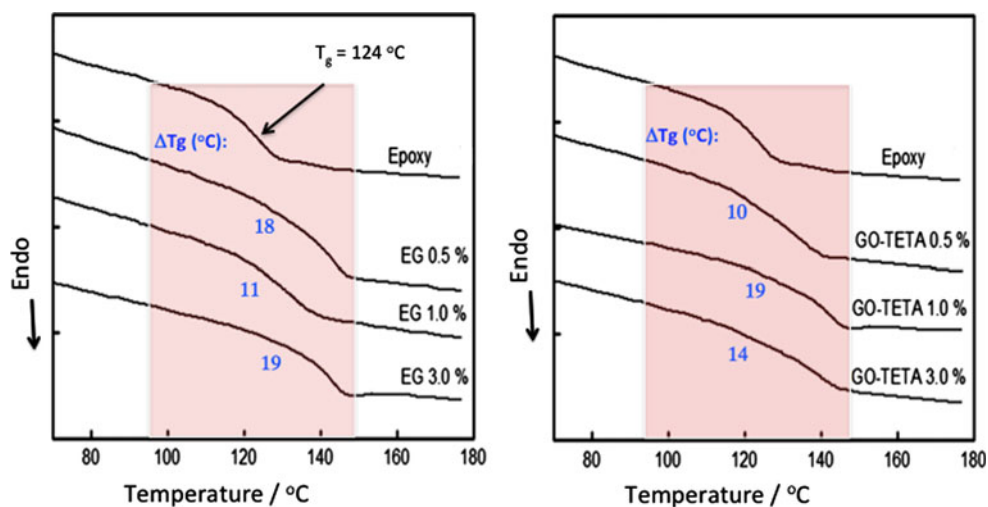


Fig. 5 SEM micrographs (thin slices prepared by ultramicrotomy) for **a** neat resin and epoxy composites with **b** 0.5 wt% of EG and **c** 3.0 wt% of GO-TETA. *Bottom* schematic of the dispersion of EG and GO-TETA in epoxy

Fig. 6 Representative DSC curves for neat epoxy, **a** epoxy/EG and **b** epoxy/GO-TETA composites; concentrations are shown in the figure. Results of the T_g increase (ΔT) determined with triplicate measures are showed in the figure



samples. The results presented in Fig. 7c, d show the elastic modulus and hardness values determined from the load–displacement curves for the neat epoxy and the 3 % composite samples at maximum depths of 300 nm, 600 nm, and 1.3 μm.

The addition of fillers to the epoxy matrix only affected the elastic modulus relative to the neat epoxy for the 3.0 wt% GO-TETA and EG samples; for the 0.5 and

1 wt% samples, the variations were within the error range. The elastic moduli of the EG composites possess a greater variability than those of the GO-TETA nanocomposites. This is likely due to the greater difficulty in uniformly dispersing the graphite sheets throughout the epoxy matrix. Sánchez et al. [31] studied epoxy nanocomposites with 1.5, 3.0, and 5.0 wt% carbon nanofiber (CNF). They obtained

Table 1 T_g values (average of three DSC measurements) and ratio elastic modulus (E)/Hardness (H) (from nanoindentation at depth of 600 nm) for neat epoxy, EG and GO-TETA-based composite samples

Samples	% w/w	T_g	$\Delta T/^\circ\text{C}$	E/H
Epoxy	0.0	124.2 \pm 0.4	0.0	7.79
EG	0.5	142.0 \pm 0.3	+17.8	7.87
	1.0	134.9 \pm 0.6	+10.7	8.49
	3.0	143.2 \pm 0.6	+19.0	8.42
	3.0	143.2 \pm 0.6	+19.0	8.42
GO-TETA	0.5	133.9 \pm 0.6	+9.7	7.84
	1.0	143.4 \pm 0.5	+19.2	8.11
	3.0	138.4 \pm 0.8	+14.2	9.15

similar results upon the addition of nanofillers to the epoxy matrix, where only the 5 wt% CNF sample exhibited a modulus higher than that of the neat resin. In 2007, Lee et al. [27] also reported no difference between the modulus values for neat epoxy samples and for samples with

0.5 wt% CNT or CNF in the epoxy matrix. Other authors have reported increases in hardness and modulus values as determined by nanoindentation upon the addition of graphene in thermoplastic polymeric matrices. Das et al. [51] observed a significant increase in both the elastic modulus and hardness upon the addition of 0.6 wt% graphene in PVA and PMMA. Shin et al. [52] reported a 286 % increase in hardness and 127 % improvement in the elastic modulus by the addition of 1.0 wt% GO modified with octyltriethoxysilane in polypropylene. Figure 7 shows that for those tests in which a maximum indentation depth of 600 nm was used, the values of the elastic modulus were quite close to those values obtained for an indentation depth of 300 nm (no significant difference); a decrease was observed for the elastic modulus of the 1.3 μm test, which was more pronounced for the composites. However, the hardness shows a significant decrease among the three depths tested. In 2003, Penumadu et al. [53] also observed a tendency of the elastic modulus and hardness of

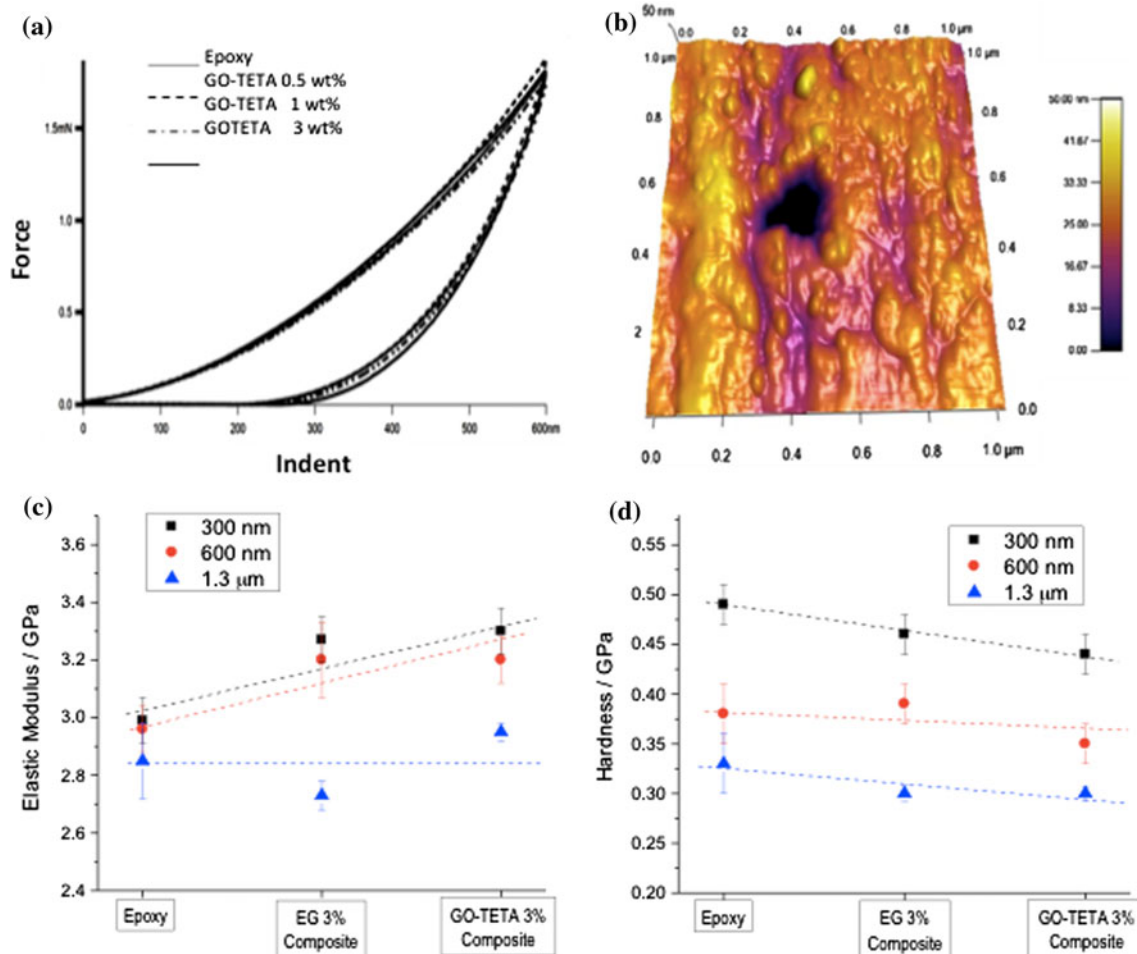
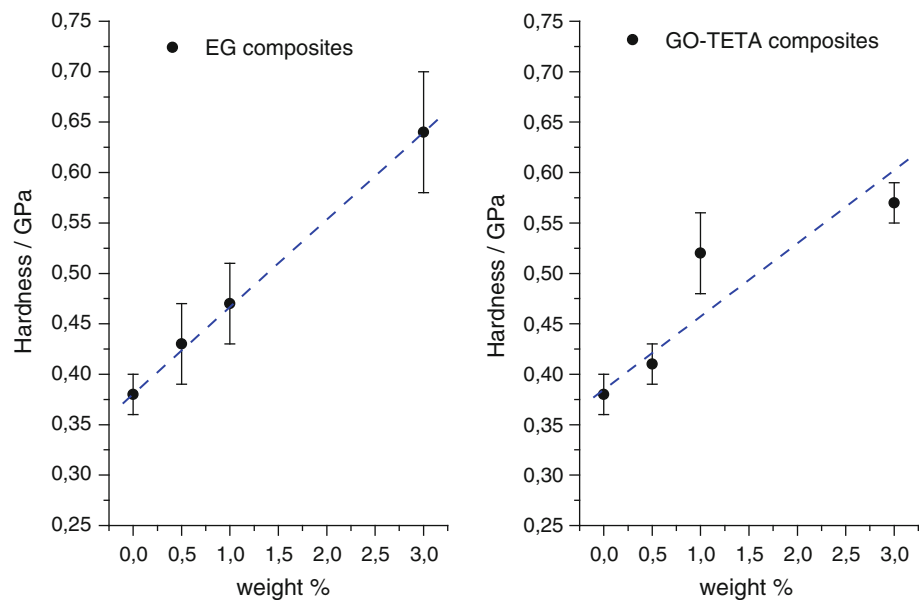


Fig. 7 **a** Typical force–displacement curve during nanoindentation of neat epoxy and epoxy/GO-TETA with concentrations of 0.5, 1.0, and 3.0 wt% nanofiller; **b** AFM micrograph showing the mark produced

by one of the indentation tests; **c** elastic modulus and **d** hardness for neat epoxy and composites with 3 wt% filler at three nanoindentation experiments with different depths: 300 nm, 600 nm, and 1.3 μm

Fig. 8 Values of hardness by Vickers microindentation for neat epoxy and nanocomposites with different concentrations of EG and GO-TETA as showed in the figure



CNT/epoxy nanocomposites to decrease as a function of depth, which explained the presence of large aggregates of the nanoreinforcements formed on the surface during sample preparation.

The nanoindentation results can also be examined by the analysis of the ratio of the elastic modulus (E)/hardness (H). Shen et al. [54] showed that this ratio can be correlated to the fracture toughness, and other authors were similarly able to calculate the fracture toughness in their experiments [52]. The results of the ratio E/H are shown in Table 1, as calculated for a depth of 600 nm. The tendency for the E/H ratio to increase was observed for all composites and was more significant for the 3 wt% GO-TETA nanocomposite.

The microindentation Vickers test performed in this work revealed opposite tendencies in comparison with the nanoindentation. The surface probed by the microindentation was at least 10^6 times higher than the one involved in the nanoindentation test. The final results in terms of microhardness are showed in Fig. 8. It was observed that the hardness values increase as a consequence of the increase in the concentration of nanofiller. The increase in hardness was of 68 % to EG and 50 % GO-TETA composites in the case of 3 wt% of nanofiller, when compared to epoxy.

Increase in hardness in carbon nanomaterials/epoxy composites has been observed before [21, 31, 55], but only through nanoindentation [31, 55] or surface [21] measurements. To the best of our knowledge is reported here for the first time microindentation (with Vickers indent) in graphene/epoxy composites. Chatterjee et al. [55] performing nanoindentation measures noted a tendency in hardness of graphene/epoxy nanocomposites to increase with the incorporation of up to 1.5 wt% of amine functionalized graphene nanoplatelets. However, a dramatic

drop in the modulus and hardness was also observed by these authors at 2.0 wt%, which was attributed to the presence of agglomeration sites within the composites.

This work showed that the study of localized mechanical properties in a micro- or nano-range can generate diverse responses which must be correlated with the microstructure of the nanocomposite and the tendency toward agglomeration of the carbon nanofiller. Microindentation involved a volume of material orders higher in magnitude than nanoindentation and showed an increase in hardness with filler content that was not revealed by the nanoindenter probe.

Conclusion

Graphene nanosheets covalently functionalized with TETA and a few layers thick were prepared and characterized with several physico-chemical techniques. Nanosheets of EG and GO-TETA were incorporated into the DGEBA/TETA system and studied as a function of the weight fraction. Increases of up to ~ 20 °C for the T_g and of 18 % for the elastic modulus/hardness ratio (associated with the fracture toughness) obtained by nanoindentation were achieved for the reinforced nanocomposites relative to the neat resin.

The hardness values through microindentation highlighted a different trend when compared with the data from nanoindentation. Microindentation hardness for composites was larger than for neat epoxy (40 % enhancement for the 1 wt% composite with GO-TETA), whereas nanoindentation hardness is almost constant for all materials (at 600 nm depth, for instance). This is probably a consequence of nanoaggregation in the microstructure. Epoxy materials

with a larger service temperature, enhancement in hardness and a slight increase in toughness were therefore obtained in this work by graphene addition.

Acknowledgements This research was supported by Petrobras. H. Ribeiro is grateful to the Brazilian agency CNPq for financial support. We thank Professor José Rubens G. Carneiro and André Bragança of Mechanical Engineering/PUC-Minas for the microindentation tests. The authors are also thankful to the Instituto Nacional de Ciência e Tecnologia em Nanomateriais de Carbono, Centro de Microscopia/UFMG and Nacional de Grafite Company (Brazil).

References

- Endo M, Strano MS, Ajayan PM (2008) *Top Appl Phys* 111(62):13
- Noorden BRV (2011) *Nature* 469:14
- Kuilla T, Bhadra S, Yao D, Kim NH, Bose S, Lee JH (2010) *Prog Polym Sci* 35:1350
- Potts JR, Dreyer DR, Bielawski CW, Ruoff RS (2011) *Polymer* 52:5
- Kuilla T, Bose S, Kumar A, Khanra P, Kim NH, Lee JH (2012) *Prog Mater Sci* 57:1061
- Brodie BC (1860) *Ann Chim Phys* 59:466
- Staudenmaier L (1898) *Ber Dtsch Chem Ges* 31:1481
- Hummers WS, Offeman RE (1958) *J Am Chem Soc* 80:1339
- Park S, Ruoff RS (2009) *Nat Nanotechnol* 4:217
- Wang G, Shen X, Wang B, Yao J, Park J (2009) *Carbon* 47:1359
- Rourke JP, Pandey PA, Moore JJ, Bates M, Kinloch IA, Young RJ et al (2011) *Angew Chem Int* 50:3173
- Wang ZW, Shirley MD, Meikle ST, Whitby RLD, Mikhailovsky SV (2009) *Carbon* 47:73
- Young RJ, Kinloch IA, Gong L, Novoselov KS (2012) *Compos Sci Technol* 72(12):1459
- Niyogi S, Bekyarova E, Itkis ME, McWilliams JL, Hamon MA, Haddon RC (2006) *J Am Chem Soc* 128:7720
- Overney RM, Buenviaje C, Luginbuhl R, Dinelli F (2000) *J Therm Anal* 59:205
- Ramanathan T, Abdala AA, Stankovich S, Dikin DA, Herrera-Alonso M, Ruoff RS et al (2008) *Nat Nanotechnol* 3:327
- Liu G, Zhang H, Zhang D, Zhang Z, An X, Yi X (2012) *J Mater Sci* 47:6891. doi:10.1007/s10853-012-6633-6
- Hu Y, Shen J, Li N, Ma H, Shi M, Yan B, Huang W, Wang W et al (2010) *Compos Sci Technol* 70:2176
- Bortz DR, Heras EG, Martin-Gullon I (2012) *Macromolecules* 45:238
- Zaman I, Phan TT, Kuan HC, Meng Q, La Bao LT, Luong L, Youssf O, Ma J (2011) *Polymer* 52:1603
- Martin-Gallego M, Hernández M, Lorenzo V, Verdejo R, Lopez-Manchado MA, Sangermano M (2012) *Polymer* 53:1831
- Putz KW, Palmeri MJ, Cohn RB, Andrews R, Brinson LC (2008) *Macromolecules* 41:6752
- Fang M, Zhang Z, Li J, Zhang H, Lu H, Yang Y (2010) *J Mater Chem* 20:9635
- Yang Z, McElrath K, Bahr J, D'Souza NA (2012) *Compos B* 43:2079
- Martin-Gallego M, Verdejo R, Lopez-Manchado M, Sangermano M (2011) *Polymer* 52(21):4664
- Briscoe BJ, Fiori L, Pelillo E (1998) *J Phys D: Appl Phys* 31:2395
- Lee H, Mall S, He P, Shi D, Narasimhadevara S, Yeo-Heung Y et al (2007) *Compos B* 38:58
- Oliver WC, Pharr GM (1992) *J Mater Res* 7:1564
- Salavagione HJ, Martínez G, Ellis G (2011) *Macromol Rapid Commun* 32:1771
- Li XF, Lau KT, Yin YS (2008) *Compos Sci Technol* 68:2876
- Sánchez M, Rams J, Campo M, Jiménez-Suárez A, Ureña A (2011) *Compos B* 42:638
- Zhang YF, Bai SL, Li XK, Zhang Z (2009) *J Polym Sci B: Polym Phys* 47:1030
- Bartolomeo P, Irigoyen M, Aragon E, Frizzi M, Perrin FX (2001) *Polym Degrad Stabil* 72(1):63
- Low IM, Shi C (1998) *J Mater Sci Lett* 17:1181. doi:10.1023/A:1006517005082
- ASTM-D 3418–82 (1988) Standard test method for transition temperatures of polymers by thermal analysis. American Society for Testing and Materials, Philadelphia, p 380
- Paredes JI, Villar-Rodil S, Solís-Fernández P, Martínez-Alonso A, Tascón JMD (2009) *Langmuir* 25:5957
- Dresselhaus MS, Jorio A, Hofmann M, Dresselhaus G, Saito R (2010) *Nano Lett* 10:751
- Guardia L, Fernandez-Merino MJ, Paredes JI, Solís-Fernandez P, Villar-Rodil S, Martínez-Alonso A et al (2011) *Carbon* 49:1653
- Ferrari AC, Meyer JC, Scardaci V, Casiraghi C, Lazzeri M, Mauri F et al (2006) *Phys Rev Lett* 97:18
- Malard LM, Nilsson J, Elias DC, Brant JC, Plentz F, Alves ES et al (2007) *Phys Rev B* 76(20):201401
- Graf D, Molitor F, Ensslin K, Stampfer C, Jungen A, Hierold C et al (2007) *Nano Lett* 7:238
- Koh YK, Bae MH, Cahill DG, Pop E (2011) *Am Chem Soc Nano* 5:269
- Jeong HK, Lee YP, Jin MH, Kim ES, Bae JJ, Lee YH (2009) *Chem Phys Lett* 470:255
- Silva WM, Ribeiro H, Seara LM, Calado HDR, Ferlauto AS, Paniago RM et al (2012) *J Braz Chem Soc* 23:1078
- Ma PC, Moa SY, Tang BZ, Kim JK (2010) *Carbon* 48:1824
- Wang H, Maiyalagan T, Wang X (2012) *ACS Catal* 2:781
- Xia W, Wang Y, Bergsträßer R, Kundu S, Muhler M (2007) *Appl Surf Sci* 254:247
- Yang DQ, Rochette JF, Sacher E (2005) *Langmuir* 21:8539
- Chiang YC, Lin WH, Chang YC (2011) *Appl Surf Sci* 257:2401
- Yang K, Gu M, Guo Y, Pan X, Mu G (2009) *Carbon* 47:1723
- Das B, Prasad KE, Ramamurty U, Rao CNR (2009) *Nanotechnology* 20:125705
- Shin KY, Hong JY, Lee S, Jang J (2012) *J Mater Chem* 22:7871
- Penumadu D, Dutta A, Pharr GM, Files B (2003) *J Mater Res* 18:1849
- Shen L, Wang L, Liu T, He C (2006) *Macromol Mater Eng* 291:1358
- Chatterjee S, Wang JW, Kuo WS, Tai NH, Salzmann C, Li WL et al (2012) *Chem Phys Lett* 531:6